Accepted Manuscript

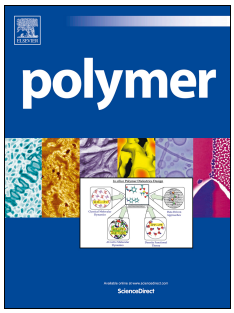

Crystallization kinetics and enhanced dielectric properties of free standing lead-free PVDF based composite films

Nan Meng, Rui Mao, Wei Tu, Katarzyna Odolczyk, Qi Zhang, Emiliano Bilotti, Michael J. Reece

PII: S0032-3861(17)30569-4

DOI: 10.1016/j.polymer.2017.06.009

Reference: JPOL 19742

To appear in: *Polymer*

Received Date: 14 April 2017

Revised Date: 25 May 2017

Accepted Date: 5 June 2017

Please cite this article as: Meng N, Mao R, Tu W, Odolczyk K, Zhang Q, Bilotti E, Reece MJ, Crystallization kinetics and enhanced dielectric properties of free standing lead-free PVDF based composite films, *Polymer* (2017), doi: 10.1016/j.polymer.2017.06.009.

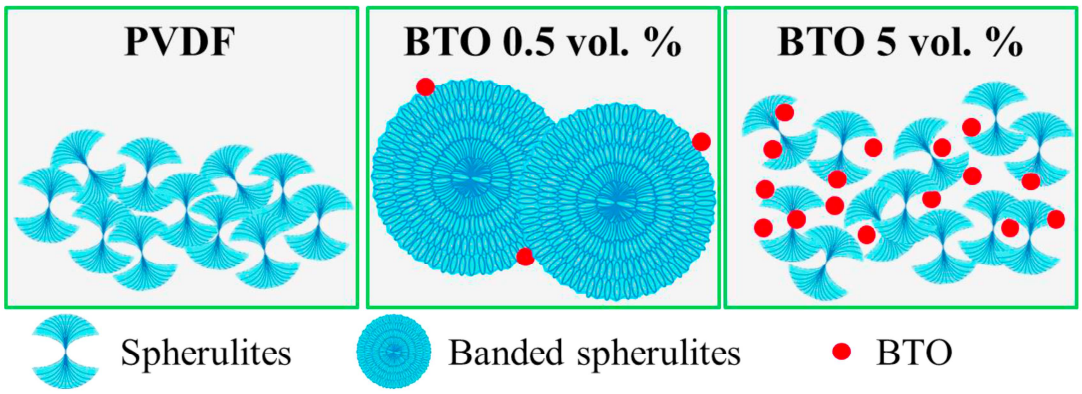

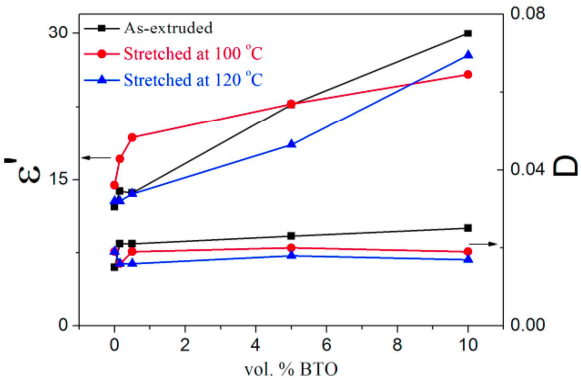

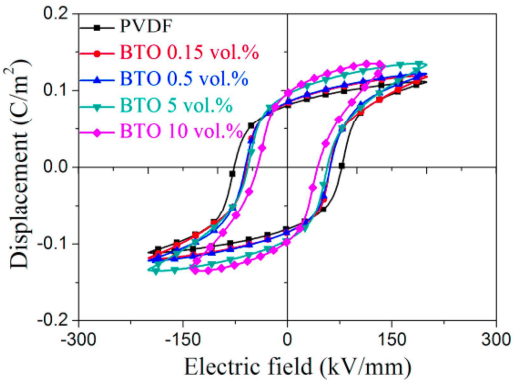

Crystallization Kinetics and Enhanced Dielectric Properties of Free Standing Lead-free PVDF Based Composite Films

Nan Meng[1], Rui Mao[1], Wei Tu[2], Katarzyna Odolczyk[3], Qi Zhang[3], Emiliano Bilotti[1, 2], Michael J. Reece[1, 2*]

[1] School of Engineering and Materials Science, and Materials Research Institute, Queen Mary University of London, Mile End Road, E1 4NS London, UK

[2] Nanoforce Technology Ltd., Joseph Priestley Building, Queen Mary University of London, Mile End Road, E1 4NS London, UK

[3] School of Aerospace, Transport and Manufacturing, Cranfield University, College Road, MK43 0AL, Cranfield, UK

Queen Mary University of London,
School of Engineering and Materials Science,
Mile End Road E1 4NS, London, UK
Tel: +44 (0)20 7882 8872; E-mail: m.j.reece@qmul.ac.uk

Key words: PVDF Composites; Crystallization kinetics; Dielectric

Abstract: Ferroelectric composites, integrating dielectric ceramic fillers with mechanically flexible polymers, are promising materials for flexible electronic applications. Plenty of research has demonstrated the enhanced dielectric and ferroelectric properties of composite materials. However, the mechanisms responsible for these enhancements are not completely understood. Herein, we used typical dielectric materials, poly(vinylidene fluoride) (PVDF) and $BaTiO_3$ (BTO), to study the effect of a dielectric filler on the crystallization, phase transformation and dielectric properties of PVDF. The crystallization of β-PVDF was not affected by the presence of BTO particles, but small amounts of BTO (< 3 vol. %) made PVDF crystallize into larger spherulites. This is linked to crystallization kinetic studies, which showed that BTO acted as a

nucleation agent for large full ring banded spherulites when its content was less than 1 vol. %. Furthermore, solid state drawing in the presence of BTO particles promoted the formation of β-PVDF with more pronounced preferred crystalline orientation at high drawing temperatures (120 °C). The dielectric and ferroelectric properties were enhanced with BTO filling. The 100 °C oriented drawn PVDF tape exhibited a dielectric permittivity of 14 (100 Hz) and remnant polarization of 0.080 C/m^2 (10 Hz), which increased to 23 and 0.095 C/m^2, respectively, after filling with 5 vol. % BTO; neither resulting in high dielectric loss tangent (~ 0.02) nor obvious current leakage. Moreover, the coercive field decreased from 80 to 50 kV/mm with increasing BTO content from 0 to 5 vol. %.

1. Introduction

The ever-increasing demand for flexible electronic devices with excellent properties, like high energy density dielectric based capacitors, can be addressed by combining dielectric ceramic fillers and polymer matrices.[1-3] Ceramic materials (e.g. barium titanate, BTO) possess large dielectric permittivity, high ferroelectric remnant polarization as well as excellent thermal stability. However, their application is impeded by their relatively low electric breakdown voltage, extreme processing conditions and high stiffness.[4] Meanwhile, polymers can be easily fabricated into complex shapes and have high break down electric fields (e.g. PVDF, > 400 kV/mm).[5] However, the intrinsic dielectric constants of polymers are a few orders of magnitude lower than those of ceramic materials (e.g. PVDF ε' ~ 10, BTO ε' ~ 900 at 1 kHz and 25 °C). Composite materials promise to integrate high dielectric constant of ceramic particles with high breakdown field and mechanically flexibility of polymers.[6,7]

In composite materials, inorganic fillers can act as nucleation sites for semi-crystalline polymers.[8,9] Dillon and co-workers[9] investigated the structure and morphology of PVDF_nanoclay composites, where the nanoclay showed an obvious nucleating effect, increasing the crystallization temperature T_c, from 125 ℃ to 145 ℃, which is consistent with the

work of Priya *et al.*[10]. Additionally, the nanoclay promoted the crystallization of the β-phase; a similar effect was also reported in PVDF composites with other inorganic fillers, e.g. BTO nanofibers,[11] functionalized BTO nanoparticles,[12] carbon nanofibers[13] and functionalized graphene sheets[14]. Apart from nucleation effects during crystallization, the presence of inorganic fillers can also influence the polymer behaviour under solid state drawing. He *et al.*[15] reported that the existence of organosilicate favoured the formation of β-PVDF during solid state drawing, which leaded to the improved piezoelectric and pyroelectric performance of PVDF_organosilicate composites.

Correlated to electric properties, Tanaka[16] put forward a multi-core model, which suggests that the characteristics of polymer chains at the interfaces differ from those in the matrix due to the adhesion between the polymer and inorganic fillers.[17] As a result, the dipoles at the interfaces can show different behaviours in comparison with those in the polymer matrix. The constituted interfacial polarization efficiently enhances the dielectric properties of composites materials.[18-20] Moreover, the properties of ferroelectric polymers are also enhanced, especially for composites loaded with small amounts of fillers.[19,21] For instance, the remnant polarization of PVDF-TrFE filled with 10.8 vol. % of BTO fibres increased to 0.093 C/m^2 from the original value of 0.047 C/m^2 for pure PVDF-TrFE.[19]

Though many studies have reported that PVDF composites exhibit improved dielectric and ferroelectric properties, the reasons for these enhancements are still not clearly understood. Moreover, the altered crystallization of the polymers and the corresponding relationship between the structure and electric properties, due to the existence of inorganic fillers, has not been comprehensively studied. Herein, we firstly report the crystallization kinetics of PVDF filled with various amounts of BTO from 0.15 to 10 vol. %, and then the impact of BTO particles on the α- to β- phase transformation of PVDF during solid state drawing. Finally, the correlation between the different crystalline features and the electric properties was analysed.

2. Material and methods

2.1 Materials

PVDF pellets were purchased from Sigma Aldrich Chemical Co. The average molecular weight of the PVDF was about 180 kg/mol (Mw) and 71 kg/mol (Mn). Tetragonal $BaTiO_3$ (BTO) particles (~ 300 nm) were purchased from Nanostructured & Amorphous Materials, Inc. The density of the PVDF and BTO particles was 1.78 and 5.85 g/cm^3, respectively, according to the suppliers. All of the materials were used without post-treatments.

2.2 Sample preparation

The PVDF_BTO composites were firstly melt-blended using an X'plore micro compounder (MC 15) at 210 ^oC and 100 rpm for 10 mins and then collected using an X'plore micro cast film line (Xplore Instruments, Geleen, The Netherlands). These extrusion conditions were found to be optimum to produce good dispersion of the BTO particles and high crystallinity of the PVDF. The volume content of BTO in the as-extruded films was varied from 0.15 to 10 vol. %. Samples of dimensions 50×15 mm^2 were cut from the as-extruded films and solid state drawn at 100 ^oC and 120 ^oC at 10 mm/min using an Instron 5900R84 machine equipped with a temperature-controlled chamber (Instron, Massachusetts, USA). The chosen drawing temperatures were appropriate to enable significant chain mobility and transform the polymer to β-phase. The draw ratio of films was calculated by dividing the extension by the original length.

The thickness of drawn films was about 25 μm, measured using a digital micrometer. Gold electrodes were evaporated on both sides of the films to enable dielectric and ferroelectric measurements.

2.3 Characterization

Phase determination of PVDF was ascertained using one-dimensional wide-angle X-ray diffraction (1D-WAXD) patterns (X'Pert Pro, PANalytical, Almelo, The Netherlands). The two-dimensional wide-angle X-ray diffraction (2D-WAXD) ring patterns were used to evaluate the

crystalline preferred orientation of composites films, which were obtained using a single crystal X-ray diffractometer (Kappa ApexII Duo, Bruker AXS GmbH, Karlsruhe, Germany) with the incident beam normal to the film surface.

The morphologies of the gold coated films were characterized using scanning electron microscopy (SEM) (FEI Inspect-F, Hillsboro, OR, USA).

The thermal behaviours (melting, crystallization and isothermal crystallization kinetics) of the PVDF_BTO composites were investigated using a differential scanning calorimeter (DSC) (DSC4000, PerkinElmer, Massachusetts, USA). Four samples of each composite material, about 5 mg, were directly cut from as-extruded or drawn films. Melting temperature and crystallinity were determined using the first heating (from 25 to 180 °C, 5 °C/min) data. The crystallization temperature was determined using the cooling (from 180-25 °C, 5 °C /min) data. The enthalpy for a fully crystalline PVDF is 104.6 J/g.[22] Isothermal crystallization was recorded at 150 °C for 15 minutes.

The fraction of ferroelectric β-phase was determined using Fourier transform infrared spectroscopy (FTIR) (Tensor 27, Bruker Optik GmbH, Ettlingen, Germany) and calculated using Equation (1) where A_α and A_β correspond to the measured absorbance at 764 cm^{-1} (α-phase) and 840 cm^{-1} (β-phase).

$$F(\beta) = \frac{A_\beta}{1.26A_\alpha + A_\beta} \qquad (1)$$

A Precision Impedance Analyser (4294A; Agilent, Santa Clara, USA) was used to test the dielectric frequency spectra at room temperature. The test frequency range was 100 Hz to 100 MHz. Ferroelectric properties were measured on a tester (NPL, Teddington, UK) at room temperature and 10 Hz.

3. Results and discussions

3.1 Effect of BTO addition on the PVDF crystallization

The 1D-XRD data of the BTO and the as-extruded films is shown in Figure 1a. The BTO powder diffraction data matches the JCPDS PDF#75-0460 data file with characteristic peaks at 2θ=44.9° (002) and 45.4° (200) and tetragonal structure (Figure 1a(1)). The diffraction peaks in Figure 1a(2) at 2θ=17.8° $(100)_\alpha$, 18.6° $(020)_\alpha$ and 20.0° $(110)_\alpha$ were assigned to the non-ferroelectric α-PVDF. The β-phase characteristic peak at 2θ=20.8°, $(110)/(200)_\beta$ reflections, could not be observed as an obvious peak, but appeared as a small shoulder in the pure PVDF and composite films, which suggests the α-phase is the predominant crystalline phase. Our previous studies showed that extruded PVDF can crystallize into small amounts of β-phase (~ 8 wt. %) as determined by FTIR technique.[22]

Figure 1b shows the surface SEM images of the as-extruded films. It suggests the good dispersion of the bright white BTO particles (~ 300 nm) in the dark grey PVDF matrix. All of the samples displayed spherulite morphology, suggesting the crystallization of α-phase, which is consistent with the XRD data (Figure 1a). Composites with BTO content of 0.15, 0.5 vol. % crystallized into larger spherulites (diameter ~ 10 μm) compared to pure PVDF (diameter ~ 3 μm). With increasing BTO content from 5 and 10 vol. %, no clear spherulite boundaries were observed and the BTO particles started to agglomerate. However, the composites showed no holes or pores, suggesting good compatibility between the BTO particles and PVDF matrix. There was no apparent preferred orientation in relation to the drawing directions for any of the films.

Figures 1c-f show DSC temperature scans and isothermal crystallization data for the as-extruded PVDF and composite films. The values of melting (T_m) and crystallization (T_c) temperatures are listed in Table 1, which also includes the crystallinity (X_c), which was determined from the

fusion enthalpy. The PVDF and composite films exhibit two fusion peaks during the first heating DSC temperature scan (Figure 1c). The lower temperature broader peak is due to the fusion of smaller and/or imperfect crystals.[22] As shown in Table 1, the position of the main fusion peak (T_m) was hardly altered by the addition of BTO particles (~ 169 °C). Similarly, a crystallinity of about 50%,[22] typical for PVDF, was found, independent of the BTO content. Figure 1d depicts the cooling DSC temperature scan after first heating. The T_c of pure PVDF was 142.1 °C, and barely varied with addition of less than 5 vol. % of BTO particles. The T_c increased to 143.5 and 146.2 °C in correspondence of 5 and 10 vol. % of BTO particles. The crystallization of semi-crystalline polymers involves two steps, crystal nucleation and crystal growth. More nucleation sites were formed with a high content of BTO (> 5 vol. %), which accelerated the crystallization of the PVDF and increased the T_c values.

Isothermal crystallization experiments were conducted to understand the effect of BTO on the crystallization of PVDF. Due to the higher T_c of the PVDF composites containing 5 and 10 vol. % BTO, the isothermal crystallization temperature was chosen as 150 °C. The time dependence of X_c for the as-extruded PVDF and composite films are shown in Figure 1e. For all of the samples, the crystallinity firstly increased with time before reaching a plateau. During isothermal crystallization at 150 °C, pure PVDF achieved up to 38% crystallinity, which is lower than that of the extruded films due to the onset crystallization temperature. Compared to the pure PVDF, the composite samples exhibited higher crystallinity regardless of filler content. The crystallinity firstly increased with increasing BTO content up to 3 vol. %, which is due to the nucleating effect of BTO particles, then decreased at higher BTO content (5 vol. % and 10 vol. %), resulting from the reduced chain mobility with a high filler content.

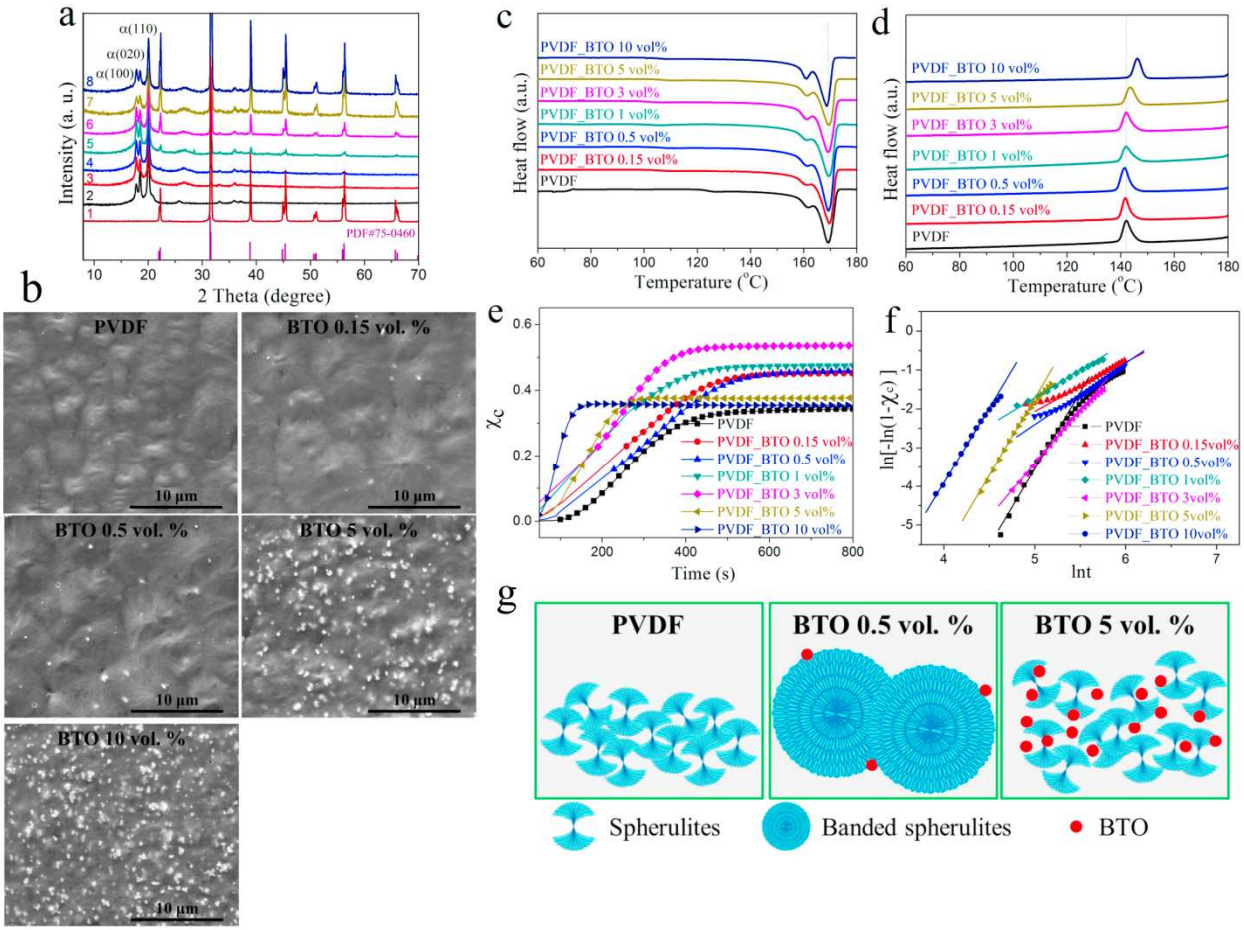

Figure 1 Crystallization features of PVDF and composites filled with different BTO content: (a) XRD patterns of: (1) BTO; (2) PVDF; (3) PVDF_BTO 0.15 vol. %; (4) PVDF_BTO 0.5 vol. %; (5) PVDF_BTO 1 vol. %; (6) PVDF_BTO 3 vol. %; (7) PVDF_BTO 5 vol. % and (8) PVDF_BTO 10 vol. %; (b) SEM images of extruded films; (c) first heating DSC temperature scan; (d) cooling DSC temperature scan; (e) crystallinity against time during isothermal crystallization at 150 °C; (f) fitted Avrami results; and (g) schematic diagrams for spherulites crystallized at 150 °C.

Another characteristic shown in Figure 1e is the reduced time needed to reach the plateau for the composites with the higher BTO contents (5 and 10 vol. %). The isothermal crystallization behaviour is well described by the Avrami equation[23], as shown in Equation (2), where X_t is the relative crystallinity at a corresponding time t, which is equal to the absolute crystallinity X_c, crystallized at time t, divided by the final maximum crystallinity; K is a constant correlated to the overall crystallization rate; n is the Avrami exponent which describes both the nucleation

nature (n_t) and crystal growth geometry (n_c) (Equation (3)). Values of K and n for PVDF and the composite films were determined by fitting the plots of ln[-ln(1- X_t)] against ln$t$ using Equation (4). The fitting curves are shown in Figure 1f and the related crystallization kinetics parameters are listed in Table 1, where the $t_{1/2}$ is defined as the required time to complete half of the crystallization, and is used to evaluate the crystallization rate.

$$X_t = 1 - \exp(-Kt^n) \quad (2)$$

$$n = n_t + n_c \quad (3)$$

$$\ln[-\ln(1 - X_t)] = \ln K + n \ln t \quad (4)$$

$$t_{1/2} = \left(\frac{\ln 2}{K}\right)^{\frac{1}{n}} \quad (5)$$

Table 1 Characteristic temperatures and thermodynamic values obtained from the DSC data. Melting temperature T_m and crystallinity X_c were determined from the first heating DSC curves; crystallization temperature T_c was determined from the cooling DSC curves and crystallinity $X_{c\text{-}iso}$, Avrami n and $t_{1/2}$ were calculated on the basis of DSC isothermal crystallization data.

Samples	T_m (°C)	X_c	T_c (°C)	$X_{c\text{-}iso}$	Avrami n	$t_{1/2}$ (s)
PVDF	168.3±1	50.7±2%	142.1±1	38.6±3%	3.8±0.1	331
BTO 0.15 vol.%	168.7±2	51.7±2%	141.7±1	45.4±2%	1.4±0.5	327
BTO 0.5 vol.%	168.9±2	52.0±3%	141.6±1	46.4±3%	1.7±0.2	344
BTO 1 vol.%	168.9±2	48.3±3%	142.0±2	47.9±1%	3.1±0.4	207
BTO 3 vol.%	168.8±1	50.0±4%	142.0±1	53.7±4%	3.6±0.2	240
BTO 5 vol.%	168.7±1	49.6±2%	143.5±1	38.0±2%	3.5±0.4	205
BTO 10 vol.%	168.6±1	50.4±2%	146.2±1	35.7±1%	3.9±0.2	136

The Avrami equation is built on the ideal assumptions of: homogenous nucleation; no change in the crystal shape; constant crystallization rate and volume of polymer; and no occurrence of secondary crystallization.[24] However, real isothermal crystallization is more complicated than this, and all of the details cannot be precisely revealed by the Avrami equation. Consequently,

the Avrami exponent *n* values, shown in Table 1, are not integers (as one would expect) and are highly scattered. Pure PVDF exhibited a value of about 4 and crystallized into spherulites (Figure 2a), indicating homogenous nucleation ($n_t = 1$) and three dimensional spherulite crystals ($n_c = 3$). The composites samples, however, showed two different behaviours. The composites filled with the lower BTO contents of 0.15, 0.5 vol. % had a *n* value of about 2, suggesting the crystallization of two-dimensional crystals ($n_c = 2$) and heterogeneous nucleation ($n_t = 0$). The *n* was in the range of 3 to 4 for composites filled with BTO contents higher than 1 vol. %, suggesting the crystallization of spherulites ($n_c = 3$) and heterogeneous nucleation ($n_t = 0$).

The morphologies of the samples crystallized at 150 °C are shown in Figure 2, where PVDF crystallized into spherulites, consistent with an Avrami exponent *n* of about 4 (Figure 2a). A similar spherulite structure was maintained for the composites filled with 0.15 vol. % of BTO particles (Figure 2b), which is contrary to the Avrami exponent *n* ranging from 1 to 2. This contradiction can be explained by the larger banded spherulites formed in the PVDF_BTO 0.5 vol. % composites, the diameter of which were about 50 μm, with concentric rings along the radial direction (Figure 2c inset). Banded spherulite structure has been reported in various semi-crystalline polymers.[25,26] The BTO particles served as nucleating agents for the crystallization of PVDF. For composites loaded with a small content of BTO fillers (up to 0.5 vol. %), the heterogeneous nucleus of inorganic particles provided enough space for the growth of the PVDF crystals, thus forming the large ring banded spherulites. The Avrami exponent *n* of PVDF_BTO 0.5 vol. % was less than 2, which is consistent with the structure of the twisted lamellae in the banded spherulites, not the spherulites themselves. With increasing BTO content, more nucleation sites were present. In this case, the crystals influenced each other and the growth of large ring banded spherulites was impeded. Correspondingly, the Avrami exponent *n* for composites with large BTO content was in the range of 3 to 4. Figure 1g schematically illustrates the different microstructures due to varying BTO content.

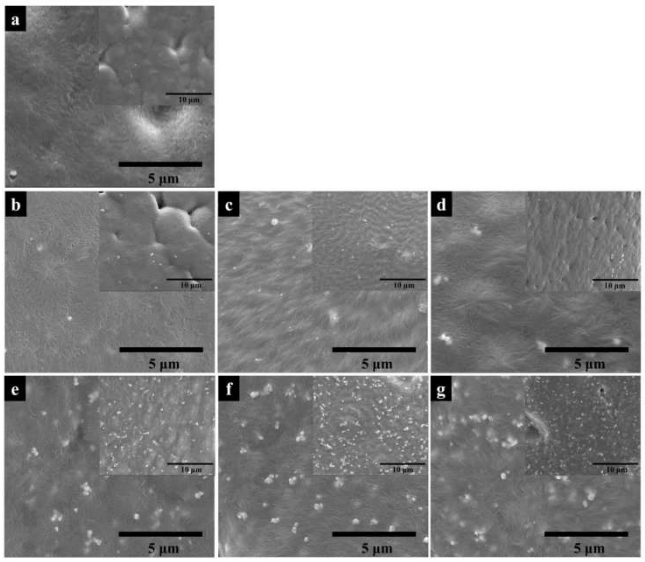

Figure 2 SEM images of samples isothermally crystallized at 150 °C: (a) pure PVDF; (b) PVDF_BTO 0.15 vol. %; (c) PVDF_BTO 0.5 vol. %; (d) PVDF_BTO 1 vol. %; (e) PVDF_BTO 3 vol. %; (f) PVDF_BTO 5 vol. %; (g) PVDF_BTO 10 vol. %.

On the basis of the $t_{1/2}$ values (Table 1), the crystallization rate of PVDF was influenced by the addition of BTO particles. Despite the nucleating effect, the $t_{1/2}$ values of composites filled with 0.15 and 0.5 vol. % BTO particles were similar to that of pure PVDF, arising from the longer time needed to the form large ring banded spherulites. With further increasing BTO content, the $t_{1/2}$ values became smaller, indicating that the addition of large amounts of BTO particles facilitated the crystallization of PVDF because there were more nucleation sites.

An important link exists between the isothermal crystallization studies and the morphology and thermal behaviours of the as-extruded films. Composites filled with less than 1 vol. % BTO particles crystallized into large ring banded spherulites (diameter ~ 50 μm) during isothermal crystallization, correspondingly, the as-extruded composites filled with the same BTO content crystallized into large spherulites (diameter ~ 10 μm), almost tripling the size of the spherulites crystallized in the pure PVDF (diameter ~ 3 μm). The introduction of a small content of BTO (up to 0.5 vol. %) reduced the amount of nucleating agent, which provided enough space for the

formation of ring banded spherulites during isothermal crystallization. However, during extrusion the crystallization of PVDF underwent rapid cooling and melt draw-down, inhibiting the formation of ring banded spherulites but still led to the crystallization of larger spherulites compared to pure PVDF.

3.2 Effect of BTO particles on solid state drawing of PVDF films

Ferroelectric β-phase PVDF is widely used in applications that require electro-active properties. The common method to obtain the β-phase is solid state drawing of α-phase PVDF with draw ratios ranging from 3 to 5. Figure S1 shows the stress-strain curves recorded during drawing of the as-extruded films, at 100 °C and 120 °C. The stretching temperatures were chosen according to the crystalline relaxation temperature of PVDF.[27] The samples showed similar values of strain at failure, ranging from 3 to 4.2, which should be sufficient to transform α- to β-phase.[28] Figure S2 shows the morphology of drawn films, which display fibrilar structure and no obvious difference exists between the 100 °C and 120 °C drawn films.

Figure 3 shows the XRD data for the drawn films. Reflections from the β-phase at 20.7° $(110)/(200)_\beta$ are clearly present (Figure 3a(i)). For the films drawn at 100 °C, the emergence of the peak at 20.7° occurred with the disappearance of the $(100)_\alpha$ peak and a reduction in the intensity of the $(110)_\alpha$ peaks. The films drawn at 120 °C clearly show combined reflections from the α- and β-phases. None of the drawn films exhibited full transformation into the β-phase, but the lower drawing temperature (100 °C) favoured this transformation, which is consistent with other reported works.[27,29,30]

The phase transformation of PVDF is induced by the uniaxial tensile deformation. Figure 3a(ii) and b(ii) depict the 2D-WAXD patterns for the films drawn to breaking point at 100 °C and 120 °C, respectively. Referenced to the 1D-XRD data, the arcs displayed in Figure 3a(ii) are attributed to the $(020)_\alpha$ and $(110)/(200)_\beta$ reflections in the 100 °C drawn PVDF films. The

equatorially concentrated (hk0) arcs indicate that the alignment of c-axis, which means the polymer chains are parallel to the drawing direction. Similarly, all of the composite samples exhibited diffraction arcs of $(100)_\alpha$, $(020)_\alpha$ and $(110)/(200)_\beta$. The full rings from the reflections of the BTO particles are progressively more obvious with increasing filler content. The degree of crystalline orientation was evaluated using the Herman's factor (f) using Equation (6), where φ is the angle between polymer chain axis and the reference direction (stretching direction), $<\cos^2\varphi>$ is defined using Equation (7) and $I(\varphi)$ is the scattered intensity along the angle φ. For ideal orientation, φ=0 and f=1.

$$f = (3<\cos^2\varphi> - 1)/2 \qquad (6)$$

$$<\cos^2\varphi> = \frac{\int_0^{\frac{\pi}{2}} I(\varphi)\sin\varphi\cos^2\varphi \mathrm{d}\varphi}{\int_0^{\frac{\pi}{2}} I(\varphi)\sin\varphi \mathrm{d}\varphi} \qquad (7)$$

The degree of orientation of the a- and b-axes of the crystallites in stretched films was calculated using the diffraction of $(100)_\alpha$, $(020)_\alpha$ and $(110)/(200)_\beta$ reflections. The unit cell of α- and β-PVDF are pseudo-orthorhombic and orthorhombic[31], respectively. In this case, the degree of orientation of the c-axis (polymer chain axis) can be derived from the relationship that exists for the a-, b-and c-axes in orthogonal crystallites (Equation (8)).

$$f_a + f_b + f_c = 0 \qquad (8)$$

The calculated f values, which represent the degree of the orientation of polymer chain axis for PVDF and the composite samples, are listed at the bottom of each 2D-WAXD pattern. The addition of BTO particles hardly influences the crystalline preferred orientation when drawing at 100 °C.

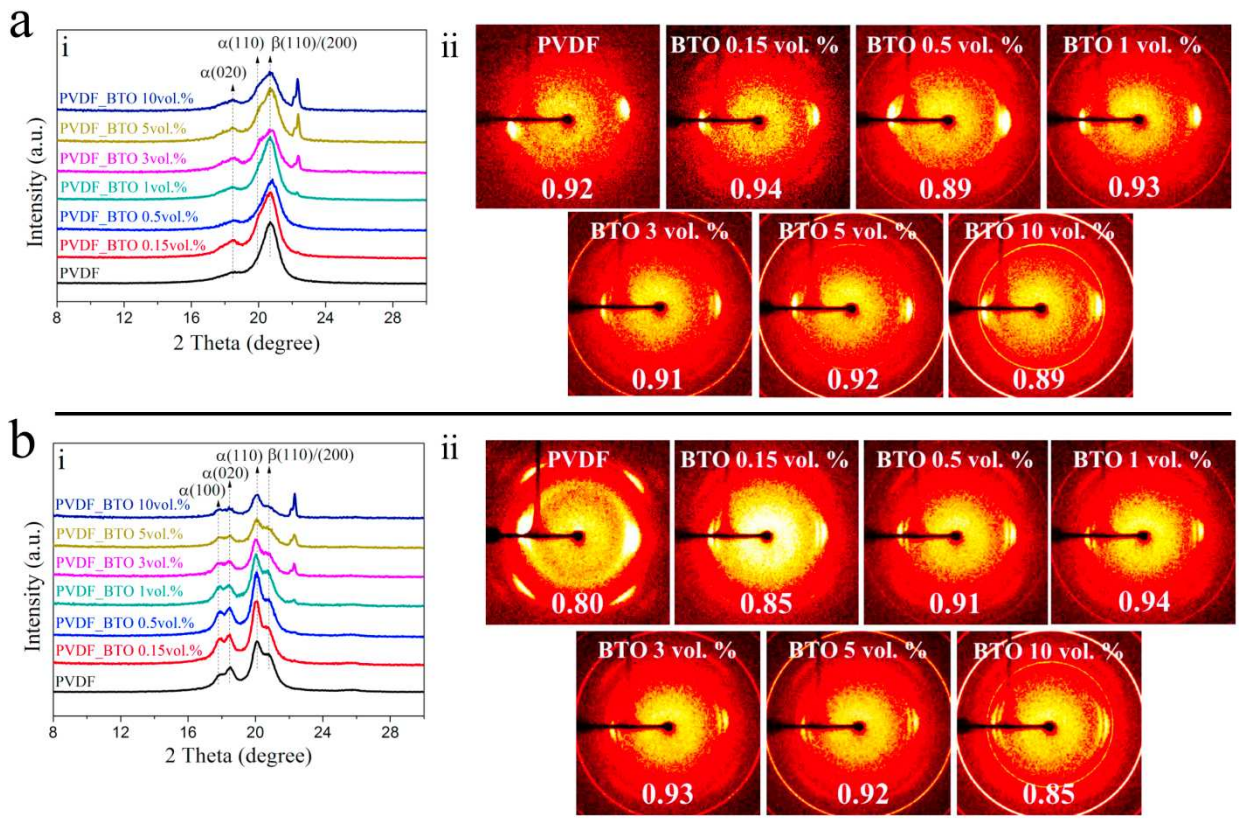

Figure 3 XRD data for films drawn to breaking point at (a) 100 °C and (b) 120 °C: (i) 1D-WAXD and (ii) 2D-WAXD; the drawing direction is vertical with the incident beam normal to the film surface and the orientation Herman's factor values were listed at the bottom of each ring pattern.

Apart from the $(020)_\alpha$ and $(110)/(200)_\beta$ reflections, the 120 °C drawn PVDF showed four arcs at about 45° off the equator, which are reflections from the $(021)_\alpha$ crystal planes. The increased chain mobility with increased temperature leads to a smaller effect of drawing on chain conformation, only orienting the crystals but not changing the chain conformation from trans-gauche to all-trans, thereby merely forming oriented α-crystals. The intensity of the $(021)_\alpha$ reflection became weaker with increasing BTO amount, which is due to the reduced α-PVDF content in the composites. Contrary to the condition of drawing at 100 °C, the degree of orientation was enhanced by the presence of BTO particles. The *f* value peaked at 0.94 for the composite filled with 1 vol. % BTO.

Figure 4a shows the DSC heating scans for the drawn films. The values of the calculated crystallinity and melting temperature are listed in Table 2. The crystallinity values represent total crystallinity of the α- and β-phases combined. Compared to the DSC graphs for the as-extruded samples, the drawn films exhibited only one fusion peak, which was about 3 °C lower than that of the main fusion peak for the as-extruded films (Figure 1c and Table 1). This is probably ascribed to the different crystalline phases; however, according to the literature the values of the melting temperature for α- and β-PVDF are possibly not differentiated.[9,32,33] The films drawn at 100 °C showed similar crystallinity to those of the as-extruded films, while the crystallinity of the films drawn at 120 °C increased moderately, which is linked to their more obvious strain hardening behaviour (Figure S1 and Table 2). Another feature shown in Figure 4a is the highly asymmetric shape of the fusion peaks for the 100 °C drawn films, owing to the heterogeneous distribution of crystallite size formed during drawing at the lower temperature,[27] which suggests strong interactions between the PVDF and BTO fillers.

Figure 4b shows the FTIR data of the drawn films. The fraction of β-phase (*F(β)*) is listed in Table 2. Films drawn at 100 °C exhibit more β-phase, which is consistent with their XRD data, and *F(β)* was nearly independent of BTO content. For films drawn at 120 °C, the formation of the β-phase was enhanced with the BTO filling. The increase was more prominent at low loadings (<5 vol. % BTO).

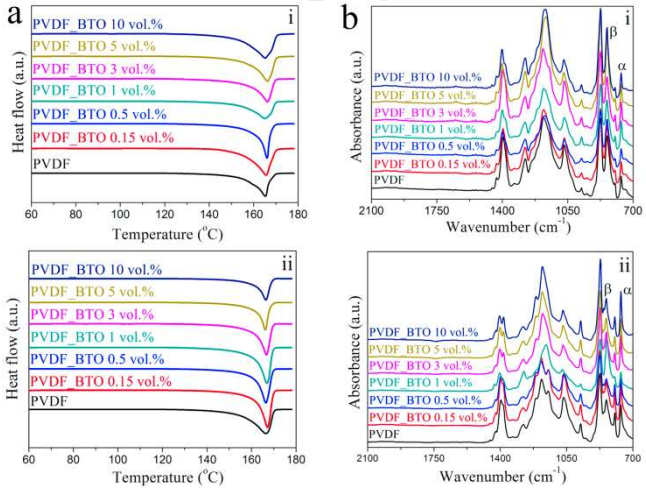

Figure 4 (a) DSC heating scans and (b) FTIR for PVDF and composite films drawn to breaking point at: (i) 100 °C; (ii) 120 °C.

Table 2 Crystallinity X_c, melting temperature T_m and fraction of β-phase $F(\beta)$ for samples drawn to maximum at 100 °C and 120 °C, the drawing rate is constant 10 mm/min.

Samples	**Drawn at 100 °C**			**Drawn at 120 °C**		
	X_c	T_m (°C)	$F(\beta)$ wt. %	X_c	T_m (°C)	$F(\beta)$ wt. %
PVDF	50.3±2%	165.5±2	86.0±4	50.7±2%	166.5±2	47.3±3
BTO 0.15 vol. %	53.5±4%	165.7±1	88.3±5	51.6±2%	167.4±1	51.4±2
BTO 0.5 vol. %	49.4±4%	166.1±2	87.2±4	52.5±2%	166.5±2	53.9±3
BTO 1 vol. %	48.8±3%	165.2±2	86.2±4	54.0±1%	166.9±1	59.9±4
BTO 3 vol. %	48.9±1%	166.3±1	83.2±5	54.8±1%	166.7±2	56.1±3
BTO 5 vol. %	49.2±4%	166.1±1	84.7±3	51.0±3%	166.1±2	51.0±3
BTO 10 vol. %	49.4±5%	165.2±2	85.1±5	51.1±3%	166.5±1	45.2±3

3.3 Electric properties of PVDF_BTO composites

Dielectric properties

The dielectric frequency spectra for the pure PVDF and the composites are shown in Figure 5a-c. In the frequency range of 100 Hz-10000 Hz, the loss tangent (D) of the as-extruded films decreased with the increase of frequency, which is ascribed to the crystalline relaxation of α-PVDF.[34]

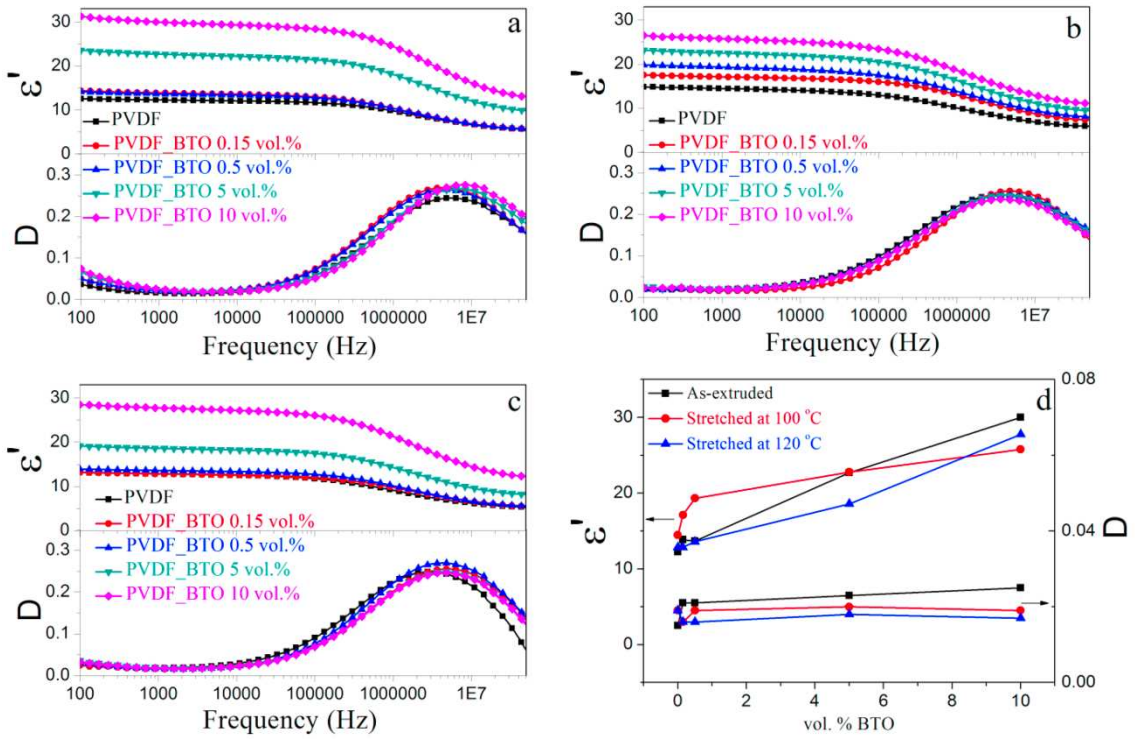

Figure 5 Frequency dependence of dielectric constant (*ε'*) and dielectric loss (*D*) of pure PVDF and composites with BTO content of 0.15, 0.5, 5, 10 vol. %: (a) as-extruded films; (b) films drawn to breaking point at 100 °C and 10 mm/min; (c) films drawn to breaking point at 120 °C and 10 mm/min. (d) values of ε' and D as a function of vol. % BTO.

Figure 5d shows the relationship between the BTO content and the values of *ε'* and *D* measured at 100 Hz and room temperature. The 100 °C drawn pure PVDF and composites with low BTO content (0.15 and 0.5 vol. %) displayed larger dielectric constant compared to the as-extruded films and the 120 °C drawn films with the same BTO content, which is due to the higher content of β-phase, consistent with the reported work by Guan *et al.* [35] Composites filled with large amounts of BTO particles (5 and 10 vol. %), however, exhibited smaller *ε'* values in the drawn samples in comparison with the as-extruded samples, which is associated with the fact that drawing reduces agglomeration of the particles and improves the distribution of high ratios of fillers. Meanwhile, the *D* did not increase obviously due to the addition of BTO particles, which proves the fact that the introduction of BTO particles did not result in severe defects, and is also

consistent with the DSC data that the composites and pure PVDF samples showed similar crystallinity values.

Ferroelectric properties

The ferroelectric properties of the pure PVDF and composites are shown in Figure 6. The displayed P-E loops are all saturated, which was determined by checking the invariance of the position of switching current peak with increasing maximum amplitude. The as-extruded samples displayed ferroelectric switching, which was associated with a field induced phase transformation during testing, from the non-polar α-phase to the polar δ-phase. The remnant polarization and coercive field for the pure as-extruded PVDF were 0.05 C/m^2 and 115 kV/mm (Figure 6a, b), respectively, consistent with the reported values for δ-PVDF.[36] Small amounts of BTO, 0.15 and 0.5 vol. %, slightly increased the remnant polarization. However, larger BTO contents, e.g. 10 vol. %, resulted in severe current leakage and decreased the breakdown voltage, which is mainly ascribed to particle aggregation and/ or the generation of defects.

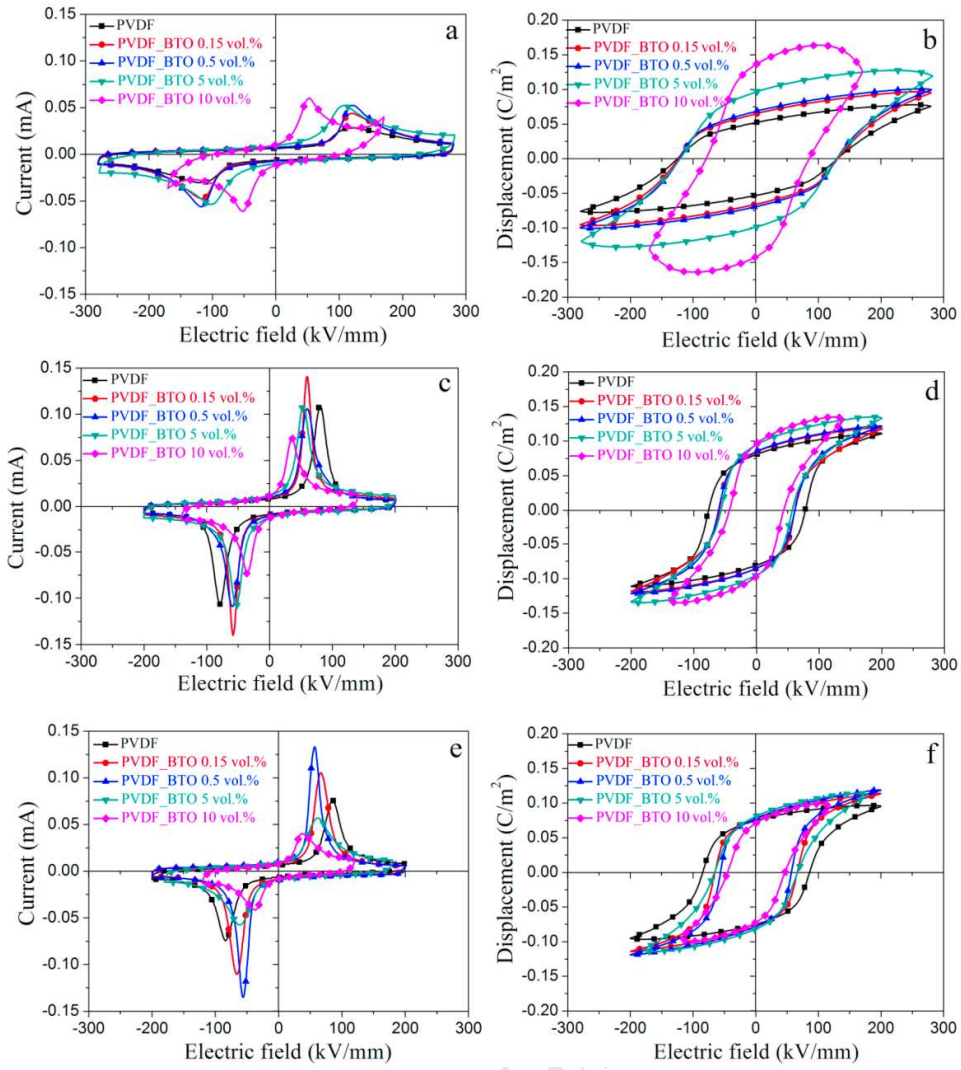

Figure 6 Ferroelectric I-E and P-E loops for pure PVDF and composites with BTO content of 0.15, 0.5, 5, and 10 vol. %: (a, b) as-extruded films; (c, d) films drawn to the limit at 100 °C and 10 mm/min; (e, f) films drawn to their breaking point at 120 °C and 10 mm/min. The data was measured at 10 Hz.

The drawn films (Figure 6c-f) produced well defined ferroelectric behaviour. The 100 °C drawn pure PVDF showed a remnant polarization of 0.080 C/m^2 and a coercive field of 80 kV/mm. Comparable values were observed in the 120 °C drawn PVDF, 0.075 C/m^2 and 86 kV/mm. The slightly lower remnant polarization in the 120 °C drawn PVDF films is linked to the lower content of the ferroelectric β-phase. It is clearly seen that the coercive field of the composites decreased to about 60 kV/mm. The interfaces between the PVDF matrix and BTO particles may have facilitated the nucleation of ferroelectric domains, which assists ferroelectric switching.[37]

For the 100 °C drawn films, the remnant polarization of the composites filled with 5 vol. % BTO reached 0.095 C/m^2, the highest value that ever reported for PVDF based composite materials, without showing any current leakage, which is ascribed to the strong adhesion between PVDF and BTO without the occurrence of particle agglomeration.

4. Conclusions

In conclusion, the PVDF/BTO composites prepared by extrusion followed by solid state drawing were systematically studied. The BTO particles do not promote the crystallization of β-phase in PVDF, but larger α-PVDF spherulites were formed with the addition of less than 3 vol. % of BTO particles. A study of isothermal crystallization revealed that small amounts of BTO produce a significant change in the crystallization behaviour of PVDF; the Avrami exponent *n* changed from 4 to 2 with the addition of small amounts of BTO (less than 1 vol. %), which indicates that the crystals of PVDF were changed from three-dimensional spherulites to two-dimensional lamellar structure due to the nucleation effect of BTO on the crystallization of large full ring banded spherulites. Additionally, in the following process of transforming α- to β-PVDF via solid state drawing, the rigid BTO particles produced stress concentrating effects along with the formation of voids and cavities, facilitating the generation of β-PVDF with more pronounced crystalline orientation in the case of the higher drawing temperature (120 °C). Finally, the dielectric properties were improved with the addition of BTO, the dielectric permittivity of 100 °C drawn films roughly increased from 14 to 23 (100 Hz), while the dielectric loss remained at about 0.02 after filling with 5 vol. % of BTO particles. The ferroelectric properties were also enhanced by drawing; the 100 °C drawn PVDF_BTO 5 vol. % composites films showed a remnant polarization of 0.095 C/m^2 the highest value ever reported for PVDF based composite materials and a coercive field of 50 kV/mm without the occurrence of obvious current leakage.

Acknowledgements: *Nan Meng* appreciates the financial support from China Scholarship Council. The authors would like to thank Dr. *Rory M Wilson* for his contributions on XRD characterization.

References

1. Z.-M. Dang, J.-K. Yuan, J.-W. Zha, T. Zhou, S.-T. Li, G.-H. Hu. *Prog Mater Sci* **2012**, *57*, 660-723.
2. Q. Wang, L. Zhu. *Journal of Polymer Science Part B: Polymer Physics* **2011**, *49*, 1421-1429.
3. K. Y. Cho, A. S. Lee, H. Jeon, S.-H. Park, M. Jang, H. G. Yoon, S. M. Hong, K.-Y. Baek, S. S. Hwang. *Polymer* **2015**, *77*, 167-176.
4. J. Y. Li, L. Zhang, S. Ducharme. *Appl Phys Lett* **2007**, *90*, 132901.
5. M. Rahimabady, S. Chen, K. Yao, F. Eng Hock Tay, L. Lu. *Appl Phys Lett* **2011**, *99*, 142901.
6. Z.-M. Dang, J.-K. Yuan, S.-H. Yao, R.-J. Liao. *Advanced Materials* **2013**, *25*, 6334-6365.
7. Prateek, V. K. Thakur, R. K. Gupta. *Chemical Reviews* **2016**, *116*, 4260-4317.
8. R. Haggenmueller, J. E. Fischer, K. I. Winey. *Macromolecules* **2006**, *39*, 2964-2971.
9. D. R. Dillon, K. K. Tenneti, C. Y. Li, F. K. Ko, I. Sics, B. S. Hsiao. *Polymer* **2006**, *47*, 1678-1688.
10. L. Priya, J. P. Jog. *Journal of Polymer Science, Part B: Polymer Physics* **2002**, *40*, 1682-1689.
11. X. Zhang, Y. Ma, C. Zhao, W. Yang. *Appl Surf Sci* **2014**, *305*, 531-538.
12. H.-J. Ye, W.-Z. Shao, L. Zhen. *J Appl Polym Sci* **2013**, *129*, 2940-2949.
13. L.-L. Sun, B. Li, Y. Zhao, W.-H. Zhong. *Polymer* **2010**, *51*, 3230-3237.
14. S. Ansari, E. P. Giannelis. *Journal of Polymer Science Part B: Polymer Physics* **2009**, *47*, 888-897.
15. F.-A. He, K. Lin, D.-L. Shi, H.-J. Wu, H.-K. Huang, J.-J. Chen, F. Chen, K.-H. Lam. *Composites Science and Technology* **2016**, *137*, 138-147.
16. T. Tanaka. *Dielectrics and Electrical Insulation, IEEE Transactions on* **2005**, *12*, 914-928.
17. T. J. Lewis. *Dielectrics and Electrical Insulation, IEEE Transactions on* **2004**, *11*, 739-753.
18. L. Shaohui, Z. Jiwei, W. Jinwen, X. Shuangxi, Z. Wenqin. *ACS Applied Materials & Interfaces* **2014**, *6*, 1533-1540.
19. Y. Song, Y. Shen, H. Liu, Y. Lin, M. Li, C.-W. Nan. *Journal of Materials Chemistry* **2012**, *22*, 8063-8068.
20. Y. Song, Y. Shen, H. Liu, Y. Lin, M. Li, C.-W. Nan. *Journal of Materials Chemistry* **2012**, *22*, 16491-16498.
21. M. Dietze, M. Es-Souni. *Sensors and Actuators A: Physical* **2008**, *143*, 329-334.
22. N. Meng, X. Zhu, R. Mao, M. J. Reece, E. Bilotti. *Journal of Materials Chemistry C* **2017**, *5*, 3296-3305.
23. M. Avrami. *The Journal of Chemical Physics* **1939**, *7*, 1103-1112.
24. M. Avrami. *The Journal of Chemical Physics* **1941**, *9*, 177-184.
25. Y. Wang, C.-M. Chan, L. Li, K.-M. Ng. *Langmuir* **2006**, *22*, 7384-7390.
26. J. Liu, H.-M. Ye, J. Xu, B.-H. Guo. *Polymer* **2011**, *52*, 4619-4630.
27. J. Defebvin, S. Barrau, G. Stoclet, C. Rochas, J.-M. Lefebvre. *Polymer* **2016**, *84*, 148-157.
28. V. Sencadas, R. Gregorio, S. Lanceros-Méndez. *Journal of Macromolecular Science, Part B* **2009**, *48*, 514-525.
29. V. R. P, D. V. Khakhar, A. Misra. *J Appl Polym Sci* **2010**, *117*, 3491-3497.
30. H.-J. Ye, L. Yang, W.-Z. Shao, S.-B. Sun, L. Zhen. *RSC Advances* **2013**, *3*, 23730-23736.
31. H. Guo, Y. Zhang, F. Xue, Z. Cai, Y. Shang, J. Li, Y. Chen, Z. Wu, S. Jiang. *CrystEngComm* **2013**, *15*, 1597-1606.
32. P. Martins, A. C. Lopes, S. Lanceros-Mendez. *Progress in Polymer Science* **2014**, *39*, 683-706.
33. E. Erdtman, K. C. Satyanarayana, K. Bolton. *Polymer* **2012**, *53*, 2919-2926.
34. T. Furukawa. *Phase Transit* **1989**, *18*, 143-211.
35. F. Guan, J. Pan, J. Wang, Q. Wang, L. Zhu. *Macromolecules* **2010**, *43*, 384-392.

36. M. Li, H. J. Wondergem, M.-J. Spijkman, K. Asadi, I. Katsouras, P. W. M. Blom, D. M. de Leeuw. *Nat Mater* **2013**, *12*, 433-438.
37. N. Meng, R. Mao, W. Tu, X. Zhu, R. M. Wilson, E. Bilotti, M. J. Reece. *Polymer* **2016**, *100*, 69-76.

Highlights

- Poly(vinylidene fluoride)/$BaTiO_3$ (PVDF/BTO) composite films were produced.
- Small amounts of BTO (< 3 vol. %) made PVDF crystallize into larger spherulites.
- BTO promoted the formation of β-PVDF during high temperature solid state drawing.
- The dielectric and ferroelectric properties were enhanced with BTO filling.